# An Experimental Test of Henry's Law in Solid Metal-Liquid Metal Systems with Implications for Iron Meteorites

**Nancy L. Chabot[1], Andrew J. Campbell[2], John H. Jones[3], Munir Humayun[2], and Carl B. Agee[4]**

[1]Geology, 112 A. W. Smith Bldg.
Case Western Reserve University
Cleveland, OH, 44106-7216
USA

(216) 368-6523
fax: (216) 368-3691
nlc9@po.cwru.edu

[2]Department of the Geophysical Sciences
The University of Chicago
5734 S. Ellis Ave.
Chicago, IL, 60637
USA

[3]Mail Code SR
NASA Johnson Space Center
Houston, TX, 77058
USA

[4]Institute of Meteoritics
Department of Earth and Planetary Sciences
University of New Mexico
Albuquerque, NM, 87131-1126
USA

Submitted to Meteoritics and Planetary Science on May 16, 2002

Revised Sept. 24, 2002

Experimental solid metal-liquid metal partition coefficients have been used to model the crystallization of magmatic iron meteorites and understand the evolution of asteroid cores. However, the majority of the partitioning experiments have been conducted with trace elements doped at levels that are orders of magnitude higher than measured in iron meteorites. Concern about Henry's Law and the unnatural doping levels have been cited as one reason why two recent iron meteorite studies have dismissed the experimental partition coefficients in their modeling. Using laser ablation ICP-MS analysis, this study reports experimentally determined solid metal-liquid metal trace element partition coefficients from runs doped down to the levels occurring in iron meteorites. The analyses for 12 trace elements (As, Co, Cr, Cu, Ga, Ge, Ir, Os, Pd, Pt, Re, and W) show no deviations from Henry's Law, and these results support decades of experimental work in which the partition coefficients were assumed to be independent of trace element concentration. Further, since our experiments are doped with natural levels of trace elements, the partitioning results are directly applicable to iron meteorites and should be used when modeling their crystallization. In contrast, our new Ag data are inconsistent with previous studies, suggesting the high Ag-content in previous studies may have influenced the measured Ag partitioning behavior.

**Introduction:**

Magmatic iron meteorites are believed to be samples of the metallic cores of asteroid-sized parent bodies. Elemental trends within each iron meteorite group are thought to result from fractional crystallization of once completely molten metallic cores (Scott, 1972). Using experimentally determined solid metal-liquid metal partition coefficients, studies have modeled the iron meteorite-forming crystallization processes inferred to have occurred early within asteroid cores (Willis and Goldstein, 1982; Jones and Drake, 1983; Haack and Scott, 1993; Ulff-Moller, 1998; Chabot and Drake, 1999).

The IIIAB group is the largest group of magmatic iron meteorites and consequently is often the focus of iron meteorite studies. Recently, Wasson (1999a) estimated the starting IIIAB core to have 2.0 wt% S based on the modal analysis of troilite nodules in large IIIAB irons, which included specifically the examination of two Cape York irons using a method similar to that of Esbensen et al. (1982). A later study revised the value slightly to 2.5 wt% S (Wasson and Richardson, 2001). However, when experimental partition coefficients and simple fractional crystallization calculations are used, other studies put the starting S-content of the IIIAB core at 10-12 wt% (Haack and Scott, 1993; Ulff-Moller, 1998; Chabot and Drake, 1999), significantly higher than the estimates based on troilite nodules. Due largely to the lower initial S-contents, the models of Wasson (1999a) and Wasson and Richardson (2001) could not reproduce the iron meteorite trends using experimental partition coefficients, and they raised the question of whether the experimental partitioning coefficients are even applicable to the crystallization of iron meteorites.

Most solid metal-liquid metal partitioning experiments have been analyzed by the electron microprobe. The electron microprobe can measure concentrations as low as 10 ppm, but

concentrations of 100 ppm or higher are preferred for reliable determinations of partition coefficients with reasonable errors. Because of the electron microprobe's detection limits, experimental samples are commonly doped with the elements of interest to near wt% levels (references in Appendix A). Such doping levels are several orders of magnitude higher than the natural elemental concentrations measured in iron meteorites. One of the reasons given by Wasson (1999a) and Wasson and Richardson (2001) for dismissing the experimental partition coefficients was concern regarding Henry's Law, suggesting the unnaturally high trace element levels affected the partitioning behavior.

It has been implicitly assumed by most experimental studies that Henry's Law considerations were less important in metallic systems than in silicate systems. In silicate systems, allowances for both the ionic size and charge of a partitioning trace element are required. Although size mismatches are important in metallic systems, charge balance is presumably not an issue. The occurrence of non-Henry's Law behavior in silicate systems has been debated, with the conclusion being that Henry's Law is satisfied over a wide range of trace element concentrations, including wt% doping levels (Beattie, 1993). A recent exception to this conclusion was reported by Bindeman and Davis (2000), who suggested that the partitioning of rare earth elements (REE), but no other trace elements, between plagioclase and silicate melt were affected by the level of REE doping. Consequently, doping at wt% levels in less-demanding, metallic systems has not been considered problematic, based on these previous experiences in silicate systems.

Solid metal-liquid metal data have not existed to evaluate whether the high doping levels have influenced the experimental partition coefficients. Using neutron activation analysis, Fleet et al. (1999) reported partition coefficients from experiments with trace elements doped as low as 50 ppm. The partitioning results were broadly consistent with previous experimental studies,

suggesting behavior that obeyed Henry's Law, but due to the varying liquid metal compositions and limited number of experiments, a rigorous test of Henry's Law could not be made.

To examine the possibility that the high trace element levels are affecting the partitioning behavior in previous studies, we experimentally determined new solid metal-liquid metal partition coefficients for Ni, P, and 13 trace elements commonly measured in iron meteorites using laser ablation ICP-MS microanalysis (Campbell and Humayun, 1999; Campbell et al., 2002). Because of the analytical sensitivity, we were able to dope our samples at lower levels than previous experimental studies, including trace element concentrations comparable to those observed in magmatic iron meteorites (Wasson, 1999a; Wasson and Richardson, 2001). With our low-level doping runs, we were able to test whether the experiments obeyed Henry's Law, with the experimental partition coefficients independent of trace element concentrations, and whether the experimental results could be applied to the crystallization of magmatic iron meteorites. Preliminary results of this study were reported by Chabot et al. (2001a, b).

**Experimental Procedure:**

All experiments were conducted by a method similar to that described in Jones and Drake (1983). Approximately 200 mg of the starting mixture was loaded into an alumina crucible and the crucible was placed in a high-purity silica tube with an inner diameter of about 9 mm. The tube was evacuated and sealed before being lowered into a Deltech vertical furnace with a $\approx$ 1.5 cm hot spot. The furnace was then ramped up to the desired temperature, which ranged from 1050 to 1470 $^{o}$C. Run durations were based on previous experimental studies (Jones and Drake, 1983; Malvin et al, 1986; Chabot and Drake, 1997, 2000) and varied from 19 days to 11 hours, depending inversely on the temperature. Runs were quenched by removing the silica tubes from

the furnace and immersing the tubes in water. Experiments were conducted at both the University of Arizona and at NASA Johnson Space Center. Two sets of experiments were conducted, one with many trace elements and varying temperature and one with fewer trace elements and varying tracer concentrations.

For the first set of experiments, mixtures of pure Fe, Ni, FeS, and P commercially available powders were used as starting materials. Thirteen trace elements were added to the experiments also as commercially purchased metal or oxide powders: Ag, As, Co, Cr, Cu, Ga, Ge, Ir, Os, Pd, Pt, Re, and W. Trace elements were added at a range of concentrations which varied between experiments and elements. The highest doping concentrations were wt% levels while the lowest doping levels were ppm. Because the starting material contained both P and S, some experiments produced two immiscible metallic liquids, one S-rich and one P-rich. Experiments with well-defined immiscible liquids yielded two separate solid metal-liquid metal partition coefficients, one for each metallic liquid. The major element compositions of runs #E2 and #E9, which contained immiscible metallic liquids, have previously been reported in Chabot and Drake (2000) along with images detailing the immiscible liquids and the Fe-P-S phase diagram.

The second set of experiments used starting mixtures of simply Fe and FeS with tracers of As, Cu, Ge, Ir, and W, added as pure, commercially purchased metal or oxide powders. For most experiments, the temperature was either 1325 or 1470 ºC. The exception is run #H6, which was run at 1455 ºC but produced a similar S-content to runs at 1470 ºC so was included in the study. Experiment #E15 was conducted at 1470 ºC and consequently was also used for comparisons. The starting concentrations of the trace elements were varied from run to run, ranging from wt% to ppm levels. Since experiments contained varied trace element concentrations but were conducted at the same temperature, occasionally multiple starting mixtures in individual capsules

were placed in a single silica tube. In these cases, about 50 mg of the starting mixture was pressed into a pellet, placed in an alumina capsule, and covered with an alumina lid. Each individual sample was approximately 3 mm tall so multiple samples could be stacked inside a silica tube and all of the runs still fell easily within the ≈1.5 cm hot spot of the furnace. When multiple capsules were present, communication between the capsules occurred via vapor transport and was more pronounced for the volatile elements As, Cu, Ge, and S than for Ir and W.

Figure 1 shows back-scattered electron (BSE) images that illustrate the variety of run products formed by the experiments. Run products were similar to those produced during previous solid metal-liquid metal partitioning studies (e.g. Chabot and Drake, 1997; 2000). The solid metal and liquid metal formed two easily distinguishable phases in the run products. The solid metal was a single homogenous phase. In contrast, the liquid metal did not form a single phase upon quenching of the experiment but rather quenched to a dendritic texture. Figure 1a and 1b show run #E11, a run which produced one of the more complicated metallic liquid quench textures of the experiments. Since run #E11 contained S as well as P, Fe-Ni dendrites were surrounded by both S-rich and P-rich phases in the quenched metallic liquid. Experiments that contained S but not P produced simpler quench textures of Fe dendrites (since these experiments were also Ni-free) surrounded by interstitial FeS, as shown in Fig. 1c and 1d. Figure 1c and 1d also illustrate that the ratio of dendrites to interstitial phases varied according to the S-content of the metallic liquid. Metallic liquids with more S contained fewer dendrites and, because of the coarser texture, a larger area of the metallic liquid was needed to obtain a representative bulk metallic liquid composition.

During the quench, dendrites commonly nucleated on the solid metal that existed at run conditions. This often created a thin "rim" of dendrites around the solid metal and a concentration of S-rich and P-rich interstitial phases adjacent to the "dendritic rim." This quenching phenomenon is illustrated in Fig. 1b and was purposely avoided during analysis of both the solid and liquid metal.

**Analytical Methods:**

Major elements, Fe, Ni, S, and P, were determined using an electron microprobe. Microprobe measurements were made with either the University of Arizona Cameca SX-50 or the NASA Johnson Space Center Cameca SX-100 instruments. Conditions of 15 kV and 20 nA were used along with a counting time of 20 sec. Due to the dendritic quench texture of the metallic liquid, multiple measurements with a 50 μm defocused beam were averaged together to get the bulk liquid composition. Averaging many measurements has been shown through image processing to accurately measure the bulk composition of similar dendritic textures (Chabot and Drake, 1997). Chabot and Drake (1997) used BSE images of S-bearing quenched metallic liquids to calculate the percentage of Fe dendrites and interstitial FeS and consequently determine the S-content of the liquid. The calculated S-content from the image analysis technique agreed with the S-content determined by averaging multiple broad beam electron microprobe measurements.

The solid metal was examined for compositional gradients using a point beam but showed no signs of inhomogeneity. Similarly, determinations of the composition of the metallic liquid were made using quenched metallic liquid from different ends of the run product, and the resulting measurements were similar and reproducible. The solid metal was also measured using both a point beam and a 50 μm defocused beam and both beam conditions gave consistent

compositional results. Errors of the solid metal are given as twice the standard deviation of multiple microprobe measurements. However, variations between individual analyses of the metallic liquid do not reflect uncertainties in the bulk composition but are rather due to the complicating dendritic quench texture. Consequently, errors given for the composition of the liquid metal are twice the standard error of the mean of multiple microprobe measurements.

Trace element concentrations were analyzed by laser ablation ICP-MS. Locations to be analyzed were first selected from BSE images acquired with an electron microprobe (Cameca SX-100, NASA Johnson Space Center) or an SEM (JEOL 5800-LV, University of Chicago). Laser ablation ICP-MS analyses were performed using a CETAC LSX-200 laser ablation peripheral with a magnetic sector ICP mass spectrometer, the Finnigan Element™, using techniques similar to those described in Campbell and Humayun (1999) and Campbell et al. (2002). The solid metal in each run was analyzed with point analyses 100 μm in diameter and 10-20 μm deep, and each point was located well within the metal grain. To minimize the effects of the quench texture, each region of quenched metallic liquid was analyzed by ablating line scans 100 μm wide, 10-20 μm deep and 500-1000 μm long. During both point and line scan analyses the mass spectrometer was swept repeatedly over the mass range of interest, and counts were accumulated at selected masses. A subset of the following isotopes was monitored during each analysis: $^{31}P$, $^{34}S$, $^{53}Cr$, $^{57}Fe$, $^{59}Co$, $^{60}Ni$, $^{63}Cu$, $^{69}Ga$, $^{74}Ge$, $^{75}As$, $^{105}Pd$, $^{107}Ag$, $^{182}W$, $^{185}Re$, $^{192}Os$, $^{193}Ir$, and $^{195}Pt$. These isotopes were chosen to maximize signal-to-noise ratios and to avoid overlap with isotopes of neighboring elements or background sources, particularly $^{16}O^{16}O$, $^{40}Ar^{14}N$, and $^{40}Ar^{16}O$. Background subtractions were performed in every case with the average of 3 blank measurements that were run immediately before and/or after each set

of analyses; the detection limit of each measurement was set as 3 standard deviations of the blank.

Instrumental sensitivity factors for each isotope relative to $^{57}Fe$ were determined by measuring signal intensity from standards (Hoba IVB, Filomena IIA, and NIST SRMs 1263a and 1158) having known concentrations of the elements of interest (Campbell et al., 2002), and the corrected intensities were normalized to 100%. Analytical precisions for each element were calculated as twice the standard error of the mean of 5 replicate analyses of each phase in each run product. The same set of instrumental sensitivity factors was used for both the solid metal and quenched metallic liquid portions of the experimental charges. The $^{34}S$ sensitivity factor was established in either of two ways: for most of the multi-element (E) runs, an average $^{34}S$ sensitivity factor was calculated using the electron microprobe results of these runs, and therefore the LA-ICP-MS results on sulfur abundances are not independent of the EMP results for these runs; for the constant temperature (H) experiments and for run #E17, a natural pyrite (Univ. of Chicago #4180) was used as an independent standard for S. When possible, elements were independently measured by both electron microprobe and laser ablation ICP-MS techniques as a test of both analytical methods. Table 1 lists the results from when there were independent analyses using both methods. There is good agreement between the results of the two analytical methods for all of the 8 elements for which such duplicate and independent measurements were available. Of particular importance is the agreement for several elements that were analyzed in the liquid by both methods; this helps to validate the use of instrumental sensitivity factors determined from metal standards for quenched metal/sulfide liquid analyses. Similar matrix insensitivity of the LA-ICP-MS technique has been noted in oxide and silicate systems (e.g., Eggins et al., 1998; Norman et al., 2002).

**Partitioning Results:**

The solid metal-liquid metal weight ratio partition coefficient (D) for an element E is calculated as:

$$D(E) = \text{wt\% E (solid metal)} / \text{wt\% E (liquid metal)} \quad [1]$$

The compositions of the individual phases in each experiment are given in Tables 2 and 3. Tables 4 and 5 list the run conditions and the partition coefficients determined in each experiment along with 2σ errors. The light element contents of the metallic liquid, such as the S, P, and C-contents, have been shown to significantly affect the solid metal-liquid metal partitioning behavior (Willis and Goldstein, 1982; Jones and Drake, 1983). To eliminate the complication of dealing with multiple light element systems, only our experimental results with less than 2 wt% P in the metallic liquid are plotted on any figures and only previous experimental data conducted in P-free and C-free systems are used for comparison. The only exception is Fig. 2b that plots our D(P) results and consequently shows experiments from P-bearing systems.

Figure 2 plots the partitioning results for Ni and P against the S-content of the metallic liquid. Previous experimental determinations of D(Ni) and D(P) are also shown (Appendix A). Nickel and P are present as major elements, doped at wt% levels, in our experiments and consequently are not part of our test of Henry's Law. However, as shown in Fig. 2, our D(Ni) and D(P) results agree well with previous measurements, giving confidence in our experiments.

Figure 3 plots our partitioning results for 12 trace elements relevant to iron meteorites against the S-content of the metallic liquid. With the exceptions of Cr and Cu, the partition coefficients increase with increasing S in the metallic liquid. The partition coefficients for Ir, Re and Os increase by nearly 3 orders of magnitude from the S-free system to compositions near the Fe-FeS eutectic. Chromium and Cu exhibit chalcophile behavior, with D(Cr) and D(Cu) decreasing with increasing S-content of the liquid.

Also plotted on Fig. 3 are previous determinations of solid metal-liquid metal partition coefficients, which, except for the neutron activation study of Fleet et al. (1999), were analyzed using the electron microprobe. Due to the detection limits of the microprobe, previous experiments were necessarily doped with near wt% levels of trace elements. In contrast, many of our experiments are doped at ppm levels, levels that are orders of magnitude lower than previous electron microprobe studies. Despite the different concentrations of trace elements, our partitioning results are consistent with the data of previous studies, as shown on Fig 3. The good agreement suggests that the trace element concentrations are not affecting the partitioning behavior and the experiments are free of deviations from Henry's Law. Additionally, our experiments complement the existing studies and, for some trace elements, significantly increase the experimental solid metal-liquid metal partitioning data available.

In contrast to the results for all the other trace elements, our partitioning results for Ag are consistently lower than the two previous Ag studies, as shown in Fig. 4. The differences between our results and previous experiments may indicate that Henry's Law is not obeyed in this instance and the high level of Ag in the previous studies may be influencing the Ag partitioning behavior. The previous Ag experiments of Chabot and Drake (1997) and Liu and Fleet (2001) were doped at high enough levels of Ag that an immiscible, pure Ag liquid was formed in the

experiments, as detailed on the Ag-Fe-S ternary diagram in Chabot and Drake (1997). The previous Ag experiments of Chabot and Drake (1997) and Liu and Fleet (2001) thus contained three phases: solid Fe-metal, S-bearing metallic liquid, and immiscible pure Ag liquid. It would not be expected that Henry's Law would be obeyed when the activity of the "trace" element is unity.

Additionally, previous Ag studies may have underestimated the Ag-content of the metallic liquid due to the complicating quench texture. This is the explanation suggested by Liu and Fleet (2001) for their inconsistencies with the work of Chabot and Drake (1997). With the presence of a pure Ag phase, it has to be decided if small Ag blebs in the metallic liquid are part of the quench texture and should be included in the analysis of the metallic liquid or if the Ag blebs represented an immiscible Ag liquid at run conditions and should be avoided during analysis.

Solid metal-liquid metal partition coefficients from experiments that contained about 2 wt% S in the metallic liquid are plotted against the concentration of the trace element in the solid metal in Fig. 5. The trace element concentration in the solid metal is used on the x-axis because magmatic iron meteorites are believed to represent the solid metal that crystallized in a molten asteroid core. As shown in Fig. 5a, from wt% to ppm trace element levels, D(As), D(Ge), and D(Ir) show no significant variations. The data for D(Cu) are more limited but also show no variation with doping level. The only previous data at 2 wt% S for these four elements are values of D(Ge) from Jones and Drake (1983), which, as shown on Fig. 5a, are also consistent with our results.

The four trace elements shown on Fig. 5a were chosen because they exhibit very different behavior as a function of S-content of the metallic liquid, from Cu being chalcophile to D(Ir) increasing by orders of magnitude with increasing S-content. Despite the different partitioning

behaviors, all four trace elements show constant partition coefficients over the doping range studied. The implication is that these four elements are representative of all of the observed trace element partitioning behaviors, and by extension all elements having partitioning behavior like one of these four are presumed also to obey Henry's Law.

It was thought that perhaps more extreme partition coefficients might be more susceptible to deviations from Henry's Law. At higher S-contents, the partition coefficients for many elements become further from unity, as seen in Fig. 3. Experiments that had a metallic liquid with about 23 wt% S are plotted in Fig. 5b against the trace element concentration in the solid metal. Our results are consistent with the previous data available at 23 wt% S (Jones and Drake, 1983; Hillgren, 1993; Appendix B). As Fig. 5b shows, even when the partition coefficients are much higher than unity, D(Ir) and D(W) show no significant variations over the three orders of magnitude range in their solid metal concentrations. In experiments doped at wt% levels, more extreme partition coefficients do not typically reflect increasing trace element concentrations in the solid metal but rather decreasing concentrations in the metallic liquid. It is thus not surprising that extreme partition coefficients also show no deviations from Henry's Law between experiments doped at wt% and ppm levels.

Further, the concentrations of As, Ge, Ir, and W in some of the experiments are at similar levels to iron meteorites, as shown by the shaded regions in Fig. 5. The partitioning values conducted at trace element levels similar to those in iron meteorites were quantitatively compared to experiments that contained higher trace element concentrations. In the unshaded region of Fig. 5a, the average value and standard deviation of D(As) is 0.33 ±0.04. The value for D(As) in the lower concentration shaded region is 0.30 ±0.05, indistinguishable statistically from the value of 0.33 ±0.04 in the unshaded region. Similarly, on Fig. 5a, D(Ge) is 0.78 ±0.06 in the

unshaded area and 0.83 ±0.06 in the shaded region, while D(Ir) is 1.65 ±0.06 in the unshaded area and 1.85 ±0.13 in the shaded region. On Fig. 5b, in the shaded area, the average partitioning value for Ir is 51 and for W is 16, which are values that are consistent with the partitioning behavior in the unshaded region, where D(Ir) is 57 ±20 and D(W) is 20 ±7.

These calculations simply illustrate quantitatively what can be seen qualitatively on Fig. 5: there is no observed significant variation in partitioning behavior as a function of trace element concentration from wt% to ppm levels. Since the experiments contain the trace elements at natural concentration levels, the experimental partition coefficients are directly applicable to iron meteorites. We also note that our results reinforce the conclusions of Jones and Malvin (1990), that the composition of the metallic liquid is the main control on the partitioning behavior.

**Iron Meteorite Implications:**

Recent iron meteorite models have advocated the importance of trapped S-rich liquid during the crystallization of asteroid cores (Wasson, 1999a; Wasson and Richardson, 2001). Metallic liquid is trapped by the crystallizing solid during iron meteorite crystallization, as evidenced by the presence of troilite-rich nodules, and determining the role that such a process plays during core crystallization deserves investigation. Wasson (1999a) chose to model the liquid trapping process quantitatively by attempting to reproduce the Ir versus As and Ir versus Au trends observed in IIIAB magmatic iron meteorites. Wasson and Richardson (2001) expanded upon and modified this work to model the IVA iron meteorite group as well. Figure 6 plots the partition coefficients used by Wasson (1999a) and Wasson and Richardson (2001) for As and Ir against the S-content of the metallic liquid. It is clear from Fig. 6 that the dependencies on S-content of both D(As) and D(Ir) from the Wasson (1999a) and Wasson and Richardson (2001) models are

not consistent with the experimental data. An abstract by Wasson (1999b) modeled the Ga and Ge IIIAB trends using a trapped melt model similar to Wasson (1999a) and also used partition coefficients that are inconsistent with the experimentally determined values.

Concern about the high doping levels of the experiments was cited as one justification for the models of Wasson (1999a) and Wasson and Richardson (2001) to use partition coefficients different from the experimental values. As our results have shown, the solid metal-liquid metal experimental data set is free from deviations from Henry's Law. The parameterization of Jones and Malvin (1990) is also shown in Fig. 6b. Our data, since they agree with the previous experimental Ir data on which the parameterization is based, fall nicely on the Jones and Malvin (1990) fit.

The Wasson (1999a) and Wasson and Richardson (2001) models differ from previous iron meteorite crystallization studies in the initial S-content of the parent bodies' cores. Since iron meteorites represent the crystallized solid metal, determining the S-content of the metallic liquid from which they crystallized is difficult and necessarily model-dependent. However, as shown on Fig. 3, the S-content of the metallic liquid has a significant effect on the partitioning behavior and consequently understanding the parent body S-content is fundamental to iron meteorite crystallization models. Wasson (1999a) and Wasson and Richardson (2001) estimated the concentration of S in the parent bodies' cores from modal analysis of troilite nodules in IIIAB and IVA iron meteorites. With the low S-contents they inferred, the experimental partition coefficients can not reproduce the IIIAB or IVA elemental trends by fractional crystallization. With higher initial S concentrations, as used by other studies (Haack and Scott, 1993; Scott et al., 1996; Ulff-Moller, 1998; Chabot and Drake, 1999), crystallization calculations based on experimental partition coefficients are able to match the general shape of the elemental

fractionations observed in magmatic iron meteorites. For example, though Haack and Scott (1993) and Chabot and Drake (1999) advocate more complicated crystallization scenarios, both studies also include model IIIAB iron meteorite trends based on just simple fractional crystallization calculations and experimental partition coefficients. Simple fractional crystallization may have difficulty reproducing the most evolved IIIAB irons, but using experimental partition coefficients, the distinctive IIIAB banana-shaped Ga and Ge trends can be reproduced, as can orders of magnitude variations in Ir (Haack and Scott, 1993; Chabot and Drake, 1999).

While matching the general shape, subtle differences between model calculations and iron meteorite trends do exist and may suggest processes more complicated than simple fractional crystallization during the solidification of asteroid cores (Haack and Scott, 1993; Ulff-Moller, 1998; Chabot and Drake, 1999). The suggestion of Wasson (1999a) and Wasson and Richardson (2001) that trapped liquid is responsible for the scatter in the crystallization trends may be correct. The evident complexities of natural processes, such as the crystallization of asteroid cores, require specifying a set of parameters for successful models that include partition coefficients, initial melt compositions (particularly S-contents), trapped liquid contents, etc. This study provides a set of experimentally determined partition coefficients relevant to modeling the natural iron meteorite system, removing the need for obtaining these by fitting the data. Using these experimentally determined partition coefficients, future models of asteroid core crystallization can better explore issues of trapped liquid content.

To summarize, with the exception of Ag, our results show that the experimental solid metal-liquid metal partition coefficients for 12 trace elements commonly analyzed in iron meteorites are consistent for trace element concentrations ranging from wt% to ppm levels. Therefore, the

experiments are free of deviations from Henry's Law. Further, the lowest trace element levels in the experiments are at similar levels to those naturally occurring in iron meteorites, making the experimental partition coefficients directly applicable to iron meteorites. These conclusions remove a large uncertainty involved in using experimental partitioning values for modeling fractional crystallization in iron meteorites. Our results indicate that Henry's Law concerns do not validate the use of partition coefficients different from those of the experimental data when modeling iron meteorite crystallization processes.

**Acknowledgements:**

This work was supported by NASA grants 344-31-20-25 to C. B. A., NAG5-9800 to M. H., RTOP 344-31-20-18 to J. H. J., NAG5-9435 to M. J. Drake, and NAG5-11122 to R. P. Harvey. N. L. C. held a National Research Council NASA-JSC Research Associateship during the majority of this work. We thank F. Ulff-Møller for motivating the early experiments and C. Schwandt for microprobe assistance. We also thank V. Lauer, A. Jurewicz, I. Casanova, and P. Jamrog for experimental and analytical assistance. We appreciate reviews by J. T. Wasson, E. B. Watson, and Associate Editor D. M. Shaw, which served to improve this manuscript.

**References:**

Beattie P. (1993) On the occurrence of apparent non-Henry's Law behaviour in experimental partitioning studies. *Geochim. Cosmochim. Acta* **57**, 47-55.

Bild R. W. and Drake M. J. (1978) Experimental investigations of trace element fractionation in iron meteorites. I – Early results. *Proc. Lunar and Planet. Sci. Conf.* **9th**, 1407-1421.

Bindeman I. N. and Davis A. M. (2000) Trace element partitioning between plagioclase and melt: Investigation of dopant influence on patition behavior. *Geochim. Cosmochim. Acta* **64**, 2863-2878.

Campbell A. J. and Humayun M. (1999) Trace element microanalysis in iron meteorites by laser ablation ICPMS. *Anal. Chem.,* 71, 939-946.

Campbell A. J., Humayun M. and Weisberg M. K. (2002) Siderophile element constraints on the formation of metal in the metal-rich chondrites Bencubbin, Weatherford, and Gujba. *Geochim. Cosmochim. Acta* **66**, 647-660.

Chabot N. L. and Drake M. J. (1997) An experimental study of silver and palladium partitioning between solid and liquid metal, with applications to iron meteorites. *Meteorit. Planet. Sci.* **32**, 637-645.

Chabot N. L. and Drake M. J. (1999) Crystallization of magmatic iron meteorites: The role of mixing in the molten core. *Meteorit. Planet. Sci.* **34**, 235-246.

Chabot N. L. and Drake M. J. (2000) Crystallization of magmatic iron meteorites: The effects of phosphorus and liquid immiscibility. *Meteorit. Planet. Sci.* **35**, 807-816.

Chabot N. L., Campbell A. J., Humayun M. and Agee C. B. (2001a) A Henry's Law test from partitioning studies of iron meteorites. In *Lunar and Planet. Sci. XXXII*, Abstract #1738, Lunar and Planetary Institute, Houston (CD-ROM).

Chabot N. L., Campbell A. J., Humayun M. and Agee C. B. (2001b) Applying experimental results to iron meteorites: A test of Henry's Law. *Meteorit. Planet. Sci* **36**, A39.

Esbensen K. H., Buchwald V. F., Malvin D. J., and Wasson J. T. (1982) Systematic compositional variations in the Cape York iron meteorite. *Geochim. Cosmochim. Acta* **46**, 1913-1920.

Eggins S. M., Rudnick R. L. and McDonough W. F. (1998) The composition of peridotites and their minerals: a laser-ablation ICP-MS study. *Earth Planet. Sci. Lett.* **154**, 53-71.

Fleet M. E. and Stone W. E. (1991) Partitioning of platinum-group elements in the Fe-Ni-S system and their fractionation in nature. *Geochim. Cosmochim. Acta* **55**, 245-253.

Fleet M. E., Liu M. and Crocket J. H. (1999) Partitioning of trace amounts of highly siderophile elements in the Fe-Ni-S system and their fractionation in nature. *Geochim. Cosmochim. Acta* **63**, 2611-2622.

Haack H. and Scott E. R. D. (1993) Chemical fractionations in group IIIAB iron meteorites: Origin by dendritic crystallization of an asteroidal core. *Geochim. Cosmochim. Acta* **57**, 3457-3472.

Hillgren V. J. (1993) Partitioning Behavior of Moderately Siderophile Elements in Ni-rich Systems: Implications for the Earth and Moon. Ph.D. thesis, University of Arizona, Tucson, Arizona, USA. 119 pp.

Hongreswat S., Chabot N. L. and Jones J. H. (2002) Modeling the solidification of magmatic iron meteorites using experimental Cu partitioning.In *Lunar and Planet. Sci. XXXIII*, Abstract #1337, Lunar and Planetary Institute, Houston (CD-ROM).

Jones J. H. and Drake M. J. (1983) Experimental investigations of trace element fractionation in iron meteorites, II: The influence of sulfur. *Geochim. Cosmochim. Acta* **47**, 1199-1209.

Jones J. H. and Malvin D. J. (1990) A nonmetal interaction model for the segregation of trace metals during solidification of Fe-Ni-S, Fe-Ni-P, and Fe-Ni-S-P alloys. *Metall. Trans. B* **21B**, 697-706.

Jones J. H. and Casanova I. (1993) Experimental partitioning of As and Sb among metal, troilite, schreibersite, barringerite, and metallic liquid. *Meteoritics* **28**, 374-375.

Jones J. H. and Jurewicz A. J. G. (1994) Partitioning of Ir, Re, and Os between solid metal and liquid metal. *EOS Trans. Am. Geophys. Union* **75**, 694-695.

Jones J. H., Hart S. R. and Benjamin T. M. (1993) Experimental partitioning studies near the Fe-FeS eutectic, with an emphasis on elements important to iron meteorite chronologies (Pb, Ag, Pd, and Tl). *Geochim. Cosmochim. Acta* **57**, 453-460.

Lauer H. V. and Jones J. H. (1998) Partitioning of Pt and Os between solid and liquid metal in Iron-Nickel-Sulfur system. In *Lunar and Planet. Sci. XXIX*, Abstract #1796, Lunar and Planetary Institute, Houston (CD-ROM).

Lauer H. V. and Jones J. H. (1999) Tungsten and Nickel partitioning between solid and liquid metal: Implications for high-pressure metal/silicate experiments. In *Lunar and Planet. Sci. XXX*, Abstract #1617, Lunar and Planetary Institute, Houston (CD-ROM).

Lauer H. V., Jones J. H. and Schwandt C. S. (2001) Influence of Carbon and Sulfur on the partitioning of Tungsten between solid and liquid metal. In *Lunar and Planet. Sci. XXXII*, Abstract #1948, Lunar and Planetary Institute, Houston (CD-ROM).

Liu M. and Fleet M. E. (2001) Partitioning of siderophile elements (W, Mo, As, Ag, Ge, Ga, and Sn) and Si in the Fe-S system and their fractionation in iron meteorites. *Geochim. Cosmochim. Acta* **65**, 671-682.

Malvin D. J., Jones J. H. and Drake M.J. (1986) Experimental investigations of trace element fractionation in iron meteorites. III: Elemental partitioning in the system Fe-Ni-S-P. *Geochim. Cosmochim. Acta* **50**, 1221-1231.

Narayan C. and Goldstein J. I. (1982) A dendritic solidification model to explain Ge-Ni variations in iron meteorite chemical groups. *Geochim. Cosmochim. Acta* **46**, 259-268.

Norman M., Robinson P. and Clark D. (2002) Major and trace element analysis of sulphide ores by laser ablation ICPMS, solution ICPMS, and XRF. *Canadian Mineral.*, in press.

Scott E. R. D. (1972) Chemical fractionation in iron meteorites and its interpretation. *Geochim. Cosmochim. Acta* **36**, 1205-1236.

Scott E. R. D., Haack H. and McCoy T. J. (1996) Core crystallization and silicate-metal mixing in the parent body of the IVA iron and stony-iron meteorites. *Geochim. Cosmochim. Acta* **60**, 1615-1631.

Ulff-Møller F. (1998) Effects of liquid immiscibility on trace element fractionation in magmatic iron meteorites: A case study of group IIIAB. *Meteorit. Planet. Sci.* **33**, 207-220.

Wasson J. T. (1999a) Trapped melt in IIIAB irons; solid/liquid elemental partitioning during the fractionation of the IIIAB magma. *Geochim. Cosmochim. Acta* **63**, 2875-2889.

Wasson J. T. (1999b) The trapped-melt model of formation for IIIAB irons Ge-Au and Ga-Au trends. In *Lunar and Planet. Sci. XXX*, Abstract #1477, Lunar and Planetary Institute, Houston (CD-ROM).

Wasson J. T. and Richardson J. W. (2001) Fractionation trends among IVA iron meteorites: Contrasts with IIIAB trends. *Geochim. Cosmochim. Acta* **65**, 951-970.

Willis J. and Goldstein J. I. (1982) The effects of C, P, and S on trace element partitioning during solidification in Fe-Ni alloys. *Proc. Lunar Planet. Sci. Conf. 13th. Part I, J. Geophys. Res.* **87**, *Supplement*, A435-A445.

**Appendix A: References for previous partitioning studies**

(just Table A1)

**Appendix B: Previously unpublished partitioning results from Jones and co-workers**

In compiling all previous 1 atm, S-bearing solid metal-liquid metal partitioning results for the trace elements in our experiments, we came across a sizeable amount of unpublished data from John Jones and co-workers over the years. Much of the unpublished data has been described qualitatively in abstract form only (Jones and Jurewicz, 1994; Jones and Casanova, 1993; Lauer and Jones, 1998,1999; Lauer et al. 2001) but the quantitative partitioning results were only available through personal communication with Jones. The unpublished data from Jones and co-workers are included on Figs. 2 and 3 as "previous data", and with the blessing of Jones, are also detailed and listed in this Appendix. The experiments in this appendix thus represent previous studies by Jones and co-workers that are completely separate from the experimental work described and presented in the main body of this paper.

The experiments presented in this Appendix were conducted and analyzed in much the same way as described by Jones and Drake (1983). Much of the data have been presented previously in abstract form: Re-Os-Ir (Jones and Jurewicz, 1994); As-Sb (Jones and Casanova, 1993); Pt-Os (Lauer and Jones, 1998); W (Lauer and Jones, 1999; Lauer et al., 2001; Jones and Drake, 1983). Tracers were added as wt% level dopants in the form of powdered metals or oxides; Ni and Fe were also added as pure metals; and S was added as natural pyrite. All charges contained enough Ni (~10 wt.%) to stabilize γ-iron (fcc structure). Charges were run in alumina crucibles within

evacuated, sealed silica tubes for durations that were inversely proportional to the run temperature. One S-free W charge was run in an alumina crucible under a flowing 90:10 mixture of Ar:$H_2$. Quenched charges were analyzed with either the Cameca Cambax or SX-100 electron microprobe at JSC. Charges from the U. of Arizona were analyzed using an ARL SEMQ. Metallic liquids were analyzed using either a defocussed or rastered beam. Experimental conditions and partitioning results are given in Table B1. Analytical and experimental uncertainty increases proportionally with increasing D. D's ≤ ~2 typically have uncertainties of ~10%, relative, or less. D's ≥ ~20 can have uncertainties of 30-50%, relative.

For all the elements investigated here, the primary control on D is the S-content of the metallic liquid. This is in agreement with previous studies (e.g., Jones and Drake, 1983; Jones and Malvin, 1990), and reinforces our confidence in the results. In fact, in one case, that of W, we have used our new data to choose among our earlier, conflicting experiments (Jones and Drake, 1983). Based on the new experiments, it seems likely that the D(W) of our old Experiment 15 was slightly high. Thus, Table B1 gives our new W data (Lauer and Jones, 1999; Lauer et al., 2001) and our preferred data from Jones and Drake (1983).

The Re-Ir-Os experiments were conducted by simultaneously doping at ~0.75 wt.% each. This was considered feasible because Jones and Drake (1983) had seen no difference in partitioning behavior (i.e., deviation from Henry's law) when multiple tracers (e.g., Ir and Au) were doped simultaneously. The results of the present study validate this approach. In this way, the uncertainties of comparing different experiments with a single tracer, performed under similar, but slightly different, conditions were largely avoided. This is an important consideration when partition coefficients become large (~≥20) and analysis of the quenched liquid (by electron microprobe) becomes difficult.

**TABLE 1.** Comparison of measurements by electron microprobe (EMP) and laser ablation (LA) ICP-MS.

| Element | Run # | EMP (wt%) | LA ICP-MS (wt%) |
|---|---|---|---|
| Cu LM | H6 | 1.1 ±0.1 | 0.98 ±0.07 |
| Cu SM | H6 | 0.6 ±0.1 | 0.54 ±0.01 |
| Ge LM | H6 | 0.88 ±0.04 | 0.80 ±0.01 |
| Ge SM | H6 | 0.6 ±0.2 | 0.69 ±0.01 |
| Ir LM | H6 | 0.75 ±0.04 | 0.72 ±0.02 |
| Ir SM | H6 | 1.3 ±0.2 | 1.20 ±0.03 |
| Ni LM | E2 | 6.6 ±0.7 | 6.0 ±0.5 |
| Ni LM | E2 | 12.1 ±0.3 | 11.6 ±0.7 |
| Ni LM | E4 | 6.7 ±0.7 | 6.2 ±0.1 |
| Ni LM | E7 | 6.1 ±0.5 | 5.6 ±0.2 |
| Ni LM | E8 | 10.3 ±0.7 | 9.3 ±0.7 |
| Ni LM | E9 | 8.7 ±1.0 | 6.8 ±0.3 |
| Ni LM | E9 | 12.6 ±0.7 | 11.7 ±1.1 |
| Ni LM | E10 | 7.1 ±0.5 | 5.8 ±0.4 |
| Ni LM | E11 | 9.2 ±0.5 | 8.6 ±0.5 |
| Ni SM | E2 | 10.7 ±0.3 | 10.3 ±0.4 |
| Ni SM | E4 | 13.5 ±0.2 | 12.8 ±0.5 |
| Ni SM | E7 | 12.0 ±0.3 | 10.9 ±0.4 |
| Ni SM | E8 | 11.9 ±0.2 | 10.7 ±0.2 |
| Ni SM | E9 | 12.5 ±0.3 | 11.7 ±0.3 |
| Ni SM | E10 | 11.0 ±0.3 | 10.2 ±0.3 |
| Ni SM | E11 | 9.5 ±0.2 | 8.9 ±0.3 |
| Os SM | E4 | 0.6 ±0.2 | 0.64 ±0.07 |
| Os SM | E8 | 1.1 ±0.4 | 1.1 ±0.1 |
| Os SM | E9 | 0.7 ±0.2 | 0.66 ±0.05 |
| Os SM | E10 | 0.7 ±0.1 | 0.67 ±0.06 |
| Os SM | E11 | 1.5 ±0.2 | 1.40 ±0.05 |
| P LM | E2 | 0.32 ±0.07 | 0.33 ±0.04 |
| P LM | E2 | 5.0 ±0.5 | 4.9 ±0.4 |
| P LM | E4 | 0.37 ±0.17 | 0.30 ±0.03 |
| P LM | E7 | 0.3 ±0.1 | 0.4 ±0.2 |
| P LM | E8 | 1.4 ±0.4 | 1.4 ±0.2 |
| P LM | E9 | 0.5 ±0.2 | 0.42 ±0.03 |
| P LM | E9 | 3.0 ±0.5 | 3.0 ±0.4 |
| P LM | E10 | 0.5 ±0.2 | 0.5 ±0.2 |
| P LM | E11 | 1.8 ±0.4 | 2.2 ±0.5 |
| P SM | E2 | 0.62 ±0.05 | 0.60 ±0.04 |
| P SM | E4 | 0.80 ±0.04 | 0.80 ±0.04 |
| P SM | E7 | 0.9 ±0.02 | 0.90 ±0.06 |
| P SM | E8 | 0.30 ±0.02 | 0.36 ±0.04 |
| P SM | E9 | 0.51 ±0.03 | 0.47 ±0.03 |
| P SM | E10 | 0.59 ±0.02 | 0.60 ±0.03 |
| P SM | E11 | 0.31 ±0.02 | 0.40 ±0.03 |
| Re LM | E2 | 0.44 ±0.07 | 0.33 ±0.03 |
| Re SM | E2 | 2.7 ±0.2 | 2.9 ±0.1 |
| S LM | H2 | 1.9 ±0.3 | 1.8 ±0.3 |
| S LM | H3 | 1.9 ±0.4 | 2.0 ±0.3 |
| S LM | H4 | 2.7 ±0.4 | 2.5 ±0.3 |
| S LM | H5 | 2.2 ±0.5 | 3.8 ±0.4 |
| S LM | H6 | 2.8 ±0.3 | 2.3 ±0.2 |
| S LM | H8 | 1.7 ±0.3 | 2.5 ±0.3 |
| S LM | H10 | 2.0 ±0.6 | 3.2 ±0.4 |
| S LM | H11_1 | 23.0 ±1.2 | 21.8 ±0.5 |
| S LM | H11_2 | 24.6 ±1.2 | 23.7 ±0.5 |
| S LM | H11_3 | 22.9 ±1.2 | 23.9 ±0.8 |
| S LM | H11_4 | 21.8 ±1.3 | 21.8 ±1.4 |
| S LM | H11_5 | 23.9 ±0.5 | 23.0 ±0.5 |

LM = liquid metal, SM = solid metal
Errors are ±2σ

**TABLE 2.** Compositions of solid and liquid metal phases in multi-element experiments.

| Run # | E2 | E2 | E4 | E7 | E8 | E9 | E9 | E10 | E11 | E14 | E15 | E16 | E17 |
|---|---|---|---|---|---|---|---|---|---|---|---|---|---|
| **Liquid metal** | | | | | | | | | | | | | |
| **Fe (wt%)** | 61.6 ±1.3* | 76.2 ±0.8* | 63.6 ±1.3 | 64.3 ±1.9 | 70.4 ±1.2 | 64.3 ±1.3* | 73.3 ±1.1* | 65.8 ±1.5 | 73.9 ±1.7 | 94.3 ±1.0 | 97.0 ±0.6 | 68.1 ±1.3 | 69.1 ±1.5 |
| **Ni (wt%)** | 6.6 ±0.7* | 12.1 ±0.3* | 6.7 ±0.7 | 6.1 ±0.5 | 10.3 ±0.7 | 8.7 ±1.0* | 12.6 ±0.7* | 7.1 ±0.5 | 9.2 ±0.5 | | | | |
| **S (wt%)** | 29.4 ±1.5* | 4.9 ±1.3* | 29.5 ±1.6 | 29.5 ±1.9 | 18.5 ±2.0 | 25.0 ±2.2* | 9.5 ±2.0* | 26.4 ±1.9 | 14.8 ±2.4 | 4.8 ±0.7 | 2.6 ±0.5 | 28.9 ±1.2 | 26.4 ±1.2 |
| **P (wt%)** | 0.32 ±0.07* | 5.0 ±0.5* | 0.37 ±0.17 | 0.25 ±0.11 | 1.4 ±0.4 | 0.5 ±0.2* | 3.0 ±0.5* | 0.5 ±0.2 | 1.8 ±0.4 | | | | |
| **Ag (ppm)** | 28000 ±6400 | 1700 ±600 | | 4300 ±570 | | 4500 ±2300 | 1000 ±500 | 5500 ±540 | 4200 ±1600 | | | | |
| **As (ppm)** | 4.0 ±1.5 | 13 ±4 | 240 ±25 | 180 ±30 | 1000 ±38 | 580 ±33 | 2000 ±180 | 580 ±40 | 1400 ±110 | 228 ±6 | 209 ±8 | 96 ±15 | 49 ±7 |
| **Co (ppm)** | 210 ±23 | 640 ±40 | 34 ±3 | 25 ±3 | 77 ±3 | 41 ±4 | 102 ±9 | 38 ±3 | 80 ±6 | 80 ±3 | 79 ±1 | 47 ±4 | 40 ±5 |
| **Cr (ppm)** | 210 ±17 | 33 ±8 | | | | | | | | 82 ±7 | 66 ±2 | 16.4 ±0.7 | |
| **Cu (ppm)** | | | 170 ±50 | 190 ±60 | 150 ±11 | 78 ±14 | 37 ±8 | 2600 ±340 | 1400 ±110 | 1020 ±50 | 500 ±20 | 3900 ±200 | 5300 ±330 |
| **Ga (ppm)** | | 2.5 ±0.9 | 15 ±5 | 14 ±6 | 252 ±8 | 34 ±5 | 260 ±28 | 59 ±10 | 500 ±60 | 13 ±1 | 35 ±1 | | |
| **Ge (ppm)** | | | | | | | | | | 22 ±1 | 30.0 ±0.6 | 1.2 ±0.2 | 1.3 ±0.3 |
| **Ir (ppm)** | | | | | | | | 1.3 ±0.7 | 63 ±7 | 11.8 ±0.6 | 17.4 ±0.8 | 0.11 ±0.03 | 0.05 ±0.02 |
| **Os (ppm)** | | | | | 340 ±16 | 8 ±2 | 410 ±50 | | 580 ±50 | 130 ±8 | 211 ±9 | 0.6 ±0.1 | 0.4 ±0.2 |
| **Pd (ppm)** | 320 ±21 | 870 ±70 | 3.8 ±0.7 | 3.5 ±0.5 | 11.2 ±0.6 | 6.1 ±0.5 | 15 ±2 | 130 ±15 | 240 ±4 | 33 ±1 | 37.4 ±0.3 | 18 ±1 | 14 ±2 |
| **Pt (ppm)** | | | | | | | | | | 16.9 ±0.7 | 23.3 ±0.9 | 0.6 ±0.1 | 0.2 ±0.1 |
| **Re (ppm)** | | 3300 ±280 | 1.9 ±0.9 | | 45 ±3 | 1.3 ±0.2 | 54 ±7 | 2.5 ±1.6 | 81 ±7 | 13.7 ±0.9 | 21.1 ±0.7 | | 0.17 ±0.07 |
| **W (ppm)** | | 5000 ±300 | 1.7 ±0.5 | | 38 ±7 | 2.5 ±0.3 | 65 ±9 | 3.3 ±1.9 | 69 ±7 | 17 ±1 | 15.8 ±0.5 | 3.5 ±0.8 | 2.3 ±0.5 |
| **Solid Metal** | | | | | | | | | | | | | |
| **Fe (wt%)** | 84.7 ±0.8* | | 85.9 ±0.6 | 88.4 ±0.4 | 87.3 ±0.8 | 84.6 ±1.2* | | 88.8 ±0.3 | 88.5 ±0.4 | 100.1 ±0.7 | 99.8 ±0.4 | 99.8 ±0.4 | 99.5 ±0.4 |
| **Ni (wt%)** | 10.7 ±0.3* | | 13.5 ±0.2 | 12.0 ±0.3 | 11.9 ±0.2 | 12.5 ±0.3* | | 11.0 ±0.3 | 9.5 ±0.2 | | | | |
| **P (wt%)** | 0.62 ±0.05* | | 0.80 ±0.04 | 0.90 ±.02 | 0.30 ±0.02 | 0.51 ±0.03* | | 0.59 ±0.02 | 0.31 ±0.02 | | | | |
| **Ag (ppm)** | 59 ±4 | | | 5.0 ±0.5 | | 14 ±1 | | 17 ±2 | 39 ±2 | | | | |
| **As (ppm)** | 5.2 ±1.4 | | 840 ±18 | 620 ±18 | 460 ±14 | 740 ±23 | | 900 ±29 | 550 ±25 | 59 ±4 | 62 ±4 | 196 ±9 | 160 ±6 |
| **Co (ppm)** | 780 ±15 | | 160 ±2 | 109 ±5 | 145 ±4 | 152 ±7 | | 145 ±6 | 138 ±4 | 85 ±5 | 81 ±4 | 190 ±10 | 210 ±10 |
| **Cr (ppm)** | 15 ±2 | | | | | | | | | 39 ±8 | 44 ±6 | | |
| **Cu (ppm)** | | | 20 ±11 | 21 ±5 | 35 ±17 | 12 ±1 | | 460 ±75 | 290 ±11 | 420 ±28 | 260 ±19 | 770 ±40 | 920 ±22 |
| **Ga (ppm)** | 7 ±1 | | 560 ±21 | 440 ±20 | 860 ±34 | 650 ±22 | | 1400 ±120 | 1410 ±33 | 15 ±2 | 32 ±3 | | |
| **Ge (ppm)** | | | | | | | | | | 21 ±3 | 28 ±3 | 33 ±4 | 68 ±3 |
| **Ir (ppm)** | | | | | | | | 570 ±25 | 1100 ±35 | 34 ±3 | 33 ±2 | 74 ±7 | 28 ±9 |
| **Os (ppm)** | | | 6400 ±700 | 2900 ±290 | 10500 ±600 | 6600 ±520 | | 6700 ±600 | 13800 ±530 | 500 ±21 | 510 ±33 | 760 ±120 | 310 ±100 |
| **Pd (ppm)** | 430 ±22 | | 8.4 ±0.3 | 6.8 ±.0.7 | 7.0 ±0.9 | 9.1 ±0.8 | | 190 ±8 | 142 ±4 | 17 ±3 | 20 ±2 | 30 ±3 | 25 ±1 |
| **Pt (ppm)** | | | | | | | | | | 25 ±2 | 25 ±2 | 67 ±3 | 44 ±4 |
| **Re (ppm)** | 29000 ±1200 | | 660 ±40 | | 1070 ±60 | 700 ±31 | | 730 ±50 | 1380 ±40 | 49 ±2 | 49 ±4 | | 37 ±11 |
| **W (ppm)** | 9000 ±370 | | 150 ±10 | | 203 ±7 | 180 ±4 | | 220 ±13 | 274 ±7 | 34 ±1 | 23.6 ±0.7 | 240 ±11 | 192 ±9 |

* Reported in Chabot and Drake (2000).

Measurements of Fe, Ni, S, and P were made using the electron microprobe. All other elements were analyzed by laser ablation ICP-MS. Errors are ±2σ.

**TABLE 3.** Compositions of solid and liquid metal phases in constant temperature experiments.

| Run # | H2 | H3 | H4 | H5 | H6 | H8 | H10 | H11_1 | H11_2 | H11_3 | H11_4 | H11_5 |
|---|---|---|---|---|---|---|---|---|---|---|---|---|
| **Liquid metal** | | | | | | | | | | | | |
| **Fe (wt%)** | 97.7 ±0.4 | 96.9 ±0.5 | 96.3 ±0.8 | 96.7 ±0.9 | 93.8 ±0.4 | 97.7 ±0.3 | 97.6 ±0.7 | 76.6 ±1.2 | 74.6 ±1.4 | 76.4 ±1.3 | 77.7 ±1.4 | 76.2 ±0.5 |
| **S (wt%)** | 1.9 ±0.3 | 1.9 ±0.4 | 2.7 ±0.4 | 2.2 ±0.5 | 2.8 ±0.3 | 1.7 ±0.3 | 2.0 ±0.6 | 23.0 ±1.2 | 24.6 ±1.2 | 22.9 ±1.2 | 21.8 ±1.3 | 23.9 ±0.5 |
| **As (ppm)** | 1000 ±70 | 195 ±7 | 41 ±2 | 45 ±1 | 9400 ±210 | 24.0 ±0.4 | 12.3 ±0.2 | | | | | |
| **Cu (ppm)** | 2100 ±90 | 1000 ±10 | 630 ±50 | 960 ±40 | 9800 ±700 | 410 ±15 | 480 ±18 | | | | | |
| **Ge (ppm)** | 1970 ±40 | 1240 ±21 | 445 ±4 | 820 ±27 | 8010 ±70 | 27.2 ±0.3 | 17.9 ±0.3 | | | | | |
| **Ir (ppm)** | 1340 ±50 | 250 ±10 | 41 ±1 | 9.0 ±0.7 | 7200 ±160 | 12.4 ±0.2 | 1.4 ±0.1 | 2.8 ±0.3 | 340 ±70 | 0.26 ±0.05 | 34 ±8 | 0.26 ±0.02 |
| **W (ppm)** | | | | | | | | 8.1 ±0.8 | 640 ±80 | 1.9 ±0.4 | 60 ±13 | 2.6 ±0.2 |
| **Solid Metal** | | | | | | | | | | | | |
| **Fe (wt%)** | 99.6 ±0.5 | 98.2 ±1.1 | 99.7 ±0.6 | 99.5 ±0.6 | 97.7 ±0.4 | 99.3 ±0.8 | 99.8 ±0.6 | 99.8 ±0.8 | 96.5 ±0.4 | 99.9 ±0.7 | 99.7 ±0.4 | 99.8 ±0.7 |
| **As (ppm)** | 370 ±25 | 73 ±2 | 15 ±1 | 14.0 ±0.5 | 2720 ±50 | 6.1 ±0.4 | 3.0 ±0.3 | | | | | |
| **Cu (ppm)** | 1500 ±120 | 550 ±16 | 340 ±13 | 480 ±11 | 5400 ±120 | 260 ±40 | 270 ±18 | | | | | |
| **Ge (ppm)** | 1540 ±24 | 1020 ±30 | 370 ±15 | 680 ±14 | 6900 ±120 | 21.9 ±0.4 | 14.3 ±0.2 | | | | | |
| **Ir (ppm)** | 2180 ±20 | 430 ±19 | 66 ±3 | 17.0 ±0.3 | 12200 ±340 | 21 ±1 | 2.6 ±0.2 | 118 ±1 | 26900 ±900 | 15.0 ±0.3 | 1560 ±70 | 11.3 ±0.2 |
| **W (ppm)** | | | | | | | | 94 ±2 | 14000 ±400 | 30.0 ±0.8 | 820 ±13 | 36.5 ±0.6 |

Measurements of Fe and S were made using the electron microprobe. All other elements were analyzed by laser ablation ICP-MS. Errors are ±2σ.

**TABLE 4.** Partitioning results for multi-element experiments.

| Run # | E2 | E2 | E4 | E7 | E8 | E9 | E9 | E10 | E11 | E14 | E15 | E16 | E17 |
|---|---|---|---|---|---|---|---|---|---|---|---|---|---|
| **Temp (°C)** | 1150 | 1150 | 1075 | 1050 | 1250 | 1200 | 1200 | 1175 | 1225 | 1425 | 1470 | 1290 | 1290 |
| **duration** | 19 d | 19 d | 14 d | 14 d | 6 d | 7 d | 7 d | 6 d | 6 d | 12 hr | 18 hr | 4 d | 6 d |
| **wt% S** | 29.4 ±1.5* | 4.9 ±1.3* | 29.5 ±1.7 | 29.5 ±1.9 | 18.5 ±2.1 | 25.0 ±2.2* | 9.5 ±2.0* | 26.4 ±1.9 | 14.8 ±2.4 | 4.8 ±0.7 | 2.6 ±0.5 | 28.9 ±1.2 | 26.4 ±1.2 |
| **wt% P** | 0.32 ±0.07* | 5.0 ±0.5* | 0.37 ±0.17 | 0.3 ±0.1 | 1.4 ±0.4 | 0.5 ±0.2* | 3.0 ±0.5* | 0.5 ±0.2 | 1.8 ±0.4 | | | | |
| **D(Ag)** | 0.0021 ±0.0005 | 0.035 ±0.013 | | 0.0011 ±0.0002 | | 0.0031 ±.0016 | 0.014 ±0.007 | 0.0030 ±0.0004 | 0.009 ±0.003 | | | | |
| **D(As)** | 1.3 ±0.6 | 0.41 ±0.17 | 3.5 ±0.4 | 3.5 ±0.6 | 0.46 ±0.02 | 1.27 ±0.08 | 0.38 ±0.04 | 1.6 ±0.1 | 0.39 ±0.03 | 0.26 ±0.02 | 0.30 ±0.02 | 2.0 ±0.3 | 3.2 ±0.5 |
| **D(Co)** | 3.7 ±0.5 | 1.2 ±0.1 | 4.7 ±0.4 | 4.3 ±0.4 | 1.9 ±0.1 | 3.8 ±0.5 | 1.5 ±0.2 | 3.8 ±0.3 | 1.72 ±0.14 | 1.06 ±0.07 | 1.03 ±0.05 | 4.0 ±0.4 | 5.2 ±0.7 |
| **D(Cr)** | 0.069 ±0.013 | 0.45 ±0.14 | | | | | | | | 0.5 ±0.1 | 0.66 ±0.09 | | |
| **D(Cu)** | | | 0.12 ±0.07 | 0.11 ±0.04 | 0.23 ±0.12 | 0.15 ±0.03 | 0.31 ±0.07 | 0.17 ±0.03 | 0.22 ±0.02 | 0.41 ±0.04 | 0.52 ±0.04 | 0.20 ±0.02 | 0.17 ±0.01 |
| **D(Ga)** | | 2.8 ±1.1 | 37 ±12 | 31 ±14 | 3.4 ±0.2 | 19 ±3 | 2.5 ±0.3 | 24 ±5 | 2.8 ±0.3 | 1.1 ±0.2 | 0.92 ±0.08 | | |
| **D(Ge)** | | | | | | | | | | 1.0 ±0.2 | 0.9 ±0.1 | 28 ±5 | 50 ±10 |
| **D(Ir)** | | | | | | | | 430 ±230 | 18 ±2 | 2.9 ±0.3 | 1.9 ±0.1 | 680 ±190 | 590 ±320 |
| **D(Ni)** | 1.6 ±0.2 | 0.90 ±0.03 | 2.0 ±0.2 | 2.0 ±0.2 | 1.2 ±0.1 | 1.4 ±0.2 | 1.0 ±0.1 | 1.6 ±0.1 | 1.0 ±0.1 | | | | |
| **D(Os)** | | | | | 31 ±3 | 880 ±280 | 16 ±2 | | 24 ±2 | 3.8 ±0.3 | 2.4 ±0.2 | 1200 ±320 | 750 ±410 |
| **D(P)** | 1.9 ±0.5 | 0.12 ±0.02 | 2 ±1 | 3.6 ±1.4 | 0.21 ±0.06 | 1.0 ±0.4 | 0.17 ±0.03 | 1.1 ±0.4 | 0.17 ±0.04 | | | | |
| **D(Pd)** | 1.3 ±0.1 | 0.50 ±0.05 | 2.2 ±0.4 | 2.0 ±0.3 | 0.63 ±0.09 | 1.5 ±0.2 | 0.6 ±0.1 | 1.4 ±0.2 | 0.60 ±0.02 | 0.5 ±0.1 | 0.54 ±0.05 | 1.7 ±0.2 | 1.8 ±0.2 |
| **D(Pt)** | | | | | | | | | | 1.50 ±0.13 | 1.05 ±0.08 | 120 ±25 | 200 ±90 |
| **D(Re)** | | 9.0 ±0.9 | 350 ±170 | | 24 ±2 | 550 ±70 | 13 ±2 | 290 ±180 | 17 ±2 | 3.6 ±0.3 | 2.3 ±0.2 | | 220 ±110 |
| **D(W)** | | 1.80 ±0.14 | 85 ±24 | | 5 ±1 | 70 ±8 | 2.8 ±0.4 | 65 ±38 | 4.0 ±0.5 | 2.0 ±0.2 | 1.5 ±0.1 | 70 ±15 | 82 ±17 |

*Reported in Chabot and Drake (2000).
Errors are ±2σ.

**TABLE 5.** Partitioning results from constant temperature experiments.

| **Run #** | **H2** | **H3** | **H4** | **H5** | **H6** | **H8** | **H10** | **H11_1** | **H11_2** | **H11_3** | **H11_4** | **H11_5** |
|---|---|---|---|---|---|---|---|---|---|---|---|---|
| **Temp (ºC)** | 1470 | 1470 | 1470 | 1470 | 1455 | 1470 | 1470 | 1325 | 1325 | 1325 | 1325 | 1325 |
| **duration** | 14 hr | 14 hr | 14 hr | 14 hr | 13 hr | 11 hr | 14 hr | 3.5 d | 3.5 d | 3.5 d | 3.5 d | 3.5 d |
| **wt% S** | 1.9 ±0.3 | 1.9 ±0.4 | 2.7 ±0.4 | 2.2 ±0.5 | 2.8 ±0.3 | 1.7 ±0.3 | 2.0 ±0.6 | 23.0 ±1.2 | 24.6 ±1.2 | 22.9 ±1.2 | 21.8 ±1.3 | 23.9 ±0.5 |
| **D(As)** | 0.37 ±0.04 | 0.37 ±.02 | 0.36 ±0.03 | 0.31 ±0.02 | 0.29 ±0.01 | 0.26 ±0.02 | 0.25 ±0.02 | | | | | |
| **D(Cu)** | 0.71 ±0.06 | 0.57 ±0.06 | 0.55 ±0.04 | 0.50 ±0.02 | 0.55 ±0.04 | 0.63 ±0.09 | 0.56 ±0.04 | | | | | |
| **D(Ge)** | 0.78 ±0.02 | 0.82 ±0.03 | 0.84 ±0.04 | 0.83 ±0.03 | 0.86 ±0.02 | 0.80 ±0.02 | 0.80 ±0.02 | | | | | |
| **D(Ir)** | 1.6 ±0.1 | 1.7 ±0.1 | 1.6 ±0.1 | 2.0 ±0.2 | 1.7 ±0.1 | 1.7 ±0.1 | 1.8 ±0.2 | 43 ±5 | 78 ±16 | 58 ±12 | 46 ±11 | 43 ±4 |
| **D(W)** | | | | | | | | 12 ±1 | 22 ±3 | 16 ±3 | 14 ±3 | 14 ±1 |

Errors are ±2σ.

**TABLE A1.** References for previous experimental solid metal-liquid metal partitioning data and number of partition coefficients per element.

| Reference | Ag | As | Co | Cr | Cu | Ga | Ge | Ir | Ni | Os | P | Pd | Pt | Re | W |
|---|---|---|---|---|---|---|---|---|---|---|---|---|---|---|---|
| Appendix B | | 3 | | | | 1 | | 8 | 35 | 18 | | | 10 | 8 | 12 |
| Bild and Drake (1978) | | | 1 | 1 | | | | | 4 | | | | | | |
| Chabot and Drake (1997) | 8 | | | | | | | | | | | 11 | | | |
| Chabot and Drake (2000) | | | | | | | | | | | 10 | | | | |
| Fleet and Stone (1991) | | | | | | | | | 5 | | | 9 | | | |
| Fleet et al. (1999) | | | | | | | | 2 | 4 | 9 | | 2 | 2 | 7 | |
| Hillgren (1993) | | | 8 | | | 6 | | | 23 | | 3 | | | | 5 |
| Hongreswat et al. (2002) | | | | | 10 | | | | 10 | | | | | | |
| Jones et al. (1993) | | | | | | | | | | | | 1 | | | |
| Jones and Drake (1983) | | | | 1 | | 3 | 16 | 7 | 27 | | 4 | | | | |
| Jones and Malvin (1990) | | | 3 | | | | 2 | 3 | 15 | | 8 | | | | |
| Liu and Fleet (2001) | 6 | 6 | | | | 6 | 6 | | | | | | | | 4 |
| Malvin et al. (1986) | | | | | | | | | | | 31 | | | | |
| Narayan and Goldstein (1982) | | | | | | | | | | | 5 | | | | |
| Willis and Goldstein (1982) | | | | | | | 2 | 2 | 8 | | 6 | | | | |

**Table B1. Jones and co-workers unpublished partitioning experiments doped at wt% levels.**

| Experiment | T(°C) | Duration (days) | wt.% S | D(Ni) | | | |
|---|---|---|---|---|---|---|---|
| **Re-Os-Ir Series** | | | | | **D(Re)** | **D(Os)** | **D(Ir)** |
| 87A | 1340 | 7 | 20.2 | 1.00 | 34 | 40 | 27 |
| 89 | 1350 | 4 | 19.2 | 1.05 | 19.7 | 24 | 15.3 |
| 92A | 1350 | 2 | 17.4 | 1.19 | 19.0 | 20.8 | 15.2 |
| 93A | 1350 | 2 | 15.2 | 1.11 | 11.4 | 14.7 | 11.2 |
| 94A | 1250 | 5 | 27.3 | 1.72 | 196 | 208 | 157 |
| 94B | 1250 | 5 | 25.0 | 1.61 | 195 | 314 | 158 |
| 95 | 1400 | 1 | 7.4 | 0.95 | 3.7 | 4.2 | 3.3 |
| 96 | 1450 | 1 | 4.1 | 0.92 | 2.5 | 2.9 | 2.4 |
| | | | | | | | |
| **As-Sb Series** | | | | | **D(As)** | **D(Sb)** | |
| 85 | 1350 | 0.7 | 11.2 | 1.02 | 0.32 | 0.09 | |
| 83 | 1250 | 3 | 27.4 | 1.56 | — | 0.13 | |
| 84 | 1250 | 3 | 24.7 | 1.47 | 0.75 | — | |
| 81 | 950 | 6 | 29.7 | 1.98 | — | 0.55 | |
| 82 | 950 | 6 | 29.3 | 2.10 | 5.0 | — | |
| | | | | | | | |
| **Pt-Os Series** | | | | | **D(Os)** | **D(Pt)** | |
| vl6m-r8 | 1269 | 3 | 24.4 | 1.24 | 86 | 19.4 | |
| vl7m*-r10 | 1218 | 4 | 27.7 | 1.83 | 439 | 157 | |
| vl6m-r10 | 1295 | 3 | 22.6 | 1.19 | 52 | 11.1 | |
| vl7m-r1 | 1347 | 2 | 13 | 1.05 | 8.5 | 2.7 | |
| vl8*m-r5 | 1371 | 2 | 10.3 | 0.94 | 6 | 1.9 | |
| vl8*m-r7 | 1385 | 2 | 7.3 | 0.96 | 3.9 | 1.6 | |
| vl8*m-r8 | 1390 | 5 | 7.3 | 0.93 | 3.9 | 1.5 | |
| vl8*m-r9 | 1399 | 2 | 5.8 | 0.93 | 3.5 | 1.5 | |
| vl9/10m-r1 | 1254 | 6 | 24.9 | 1.34 | 65 | 45 | |
| vl7m-r8 | 1256 | 13 | 22.5 | 1.24 | 41 | 16.1 | |
| | | | | | | | |
| **W-Series** | | | | | **D(W)** | | |
| vl1-r9 | 1245 | 4 | 23.2 | 1.34 | 27 | | |
| vl1-r7 | 1276 | 7 | 24.4 | 1.38 | 24 | | |
| vl1-r6 | 1329 | 4 | 18.0 | 1.18 | 5.9 | | |
| vl2-r4 | 1240 | 7 | 15.6 | 1.12 | 13.4 | | |
| vl1-r4 | 1318 | 4 | 20.7 | 1.24 | 8.3 | | |
| vl1-r2 | 1254 | 3 | 26.1 | 1.59 | 60 | | |
| vl1-r5 | 1283 | 5 | 23.7 | 1.43 | 20.6 | | |
| 21-C[A] | 1350 | 5 | 10.7 | 0.96 | 2.8 | | |
| 21-D[A] | 1350 | 5 | 10.2 | 1.0 | 2.5 | | |
| 21-G[A] | 1250 | 10 | 19.1 | 1.22 | 20.6 | | |
| 21-H[A] | 1250 | 10 | 24.1 | 1.42 | 30 | | |
| | | | | | | | |
| | | | | | **D(W)** | **D(Ga)** | |
| Jam-2[A] | 1495 | 3 | 0 | 0.84 | 0.9 | 0.9 | |

[A]Experiment conducted at the University of Arizona.

**Figure Captions:**

**Fig. 1.** BSE images illustrate the typical features and textures of the experimental run products. **a.** Run #E11. Experiments consisted of clearly separated solid metal and liquid metal phases at run conditions. The solid metal was homogenous but the liquid metal did not remain a single phase upon quenching of the experiments. **b.** Run #E11. A higher resolution BSE image of one of the more complicated metallic liquid quench textures of the experiments is shown. The quench texture consisted of Fe-Ni dendrites (light gray) surrounded by P-rich (medium gray) and S-rich (dark gray) interstitial phases. **c.** Run #E16. Quenched metallic liquids with high S-contents contained fewer dendrites, and many microprobe measurements were needed to accurately determine the bulk liquid composition. **d.** Run #H4. Low S-content metallic liquids quenched to more uniform dendritic textures.

**Fig. 2.** The solid metal-liquid metal partition coefficients for **a.** Ni and **b.** P are plotted against the S-content of the metallic liquid. Error bars are 2σ. Nickel and P were present at wt% levels in the experiments and consequently were not used to test Henry's Law. Our determinations of D(Ni) and D(P) are in good agreement with previous work, references for which are given in Appendix A.

**Fig. 3.** Solid metal-liquid metal partition coefficients for **a.** As, **b.** Co, **c.** Cr, **d.** Cu, **e.** Ga, **f.** Ge, **g.** Ir, **h.** Os, **i.** Pd, **j.** Pt, **k.** Re, and **l.** W are plotted against the S-content of the metallic liquid. Though our experiments are doped at lower levels than previous studies, our partitioning results for all 12 elements are in good agreement with the previous data, indicating that the

experimental data are free from deviations from Henry's Law. Error bars are 2σ and references for previous studies are given in Appendix A.

**Fig. 4.** Unlike the other 12 trace elements plotted in Fig. 3, our D(Ag) results are not in agreement with the work of the two previous experimental studies, all of which are plotted with 2σ error bars. The inconsistencies could indicate a deviation from Henry's Law due to the higher trace amounts of Ag in the previous experiments. The previous experiments contained enough Ag to form a pure Ag immiscible metallic liquid in the runs.

**Fig. 5.** Solid metal-liquid metal partition coefficients from experiments conducted at constant S-contents of either **a.** 2 wt% S or **b.** 23 wt% S are plotted against the trace element concentration in the solid metal, with 2σ error bars. No significant, systematic variation with trace element concentration is observed for any of the 5 elements, despite their very different partitioning dependencies on S-content. Extreme partition coefficients that are much different than unity, such as D(Ir) at 23 wt% S, also show no variation with doping levels that span three orders of magnitude. Further, some of the experiments contain trace elements at levels comparable to those in magmatic iron meteorites, as denoted by the shaded region. These results directly test Henry's Law and show that the experimental data are unaffected by doping levels ranging from wt% to ppm and the partition coefficients are applicable to iron meteorites.

**Fig. 6.** Solid metal-liquid metal partition coefficients for **a.** As and **b.** Ir are plotted against the S-content of the metallic liquid and compared to the partition coefficients used in recent iron meteorite crystallization models. The models of Wasson (1999a) and Wasson and Richardson

(2001) do not reproduce the partitioning dependency of either As or Ir on the S-content of the metallic liquid. The parameterization of D(Ir) by Jones and Malvin is in good agreement with the general trend of the experimental data. Our results have shown that the experimental data is free of deviations from Henry's Law, and such concerns do not justify using partition coefficients that differ from the experimental values.

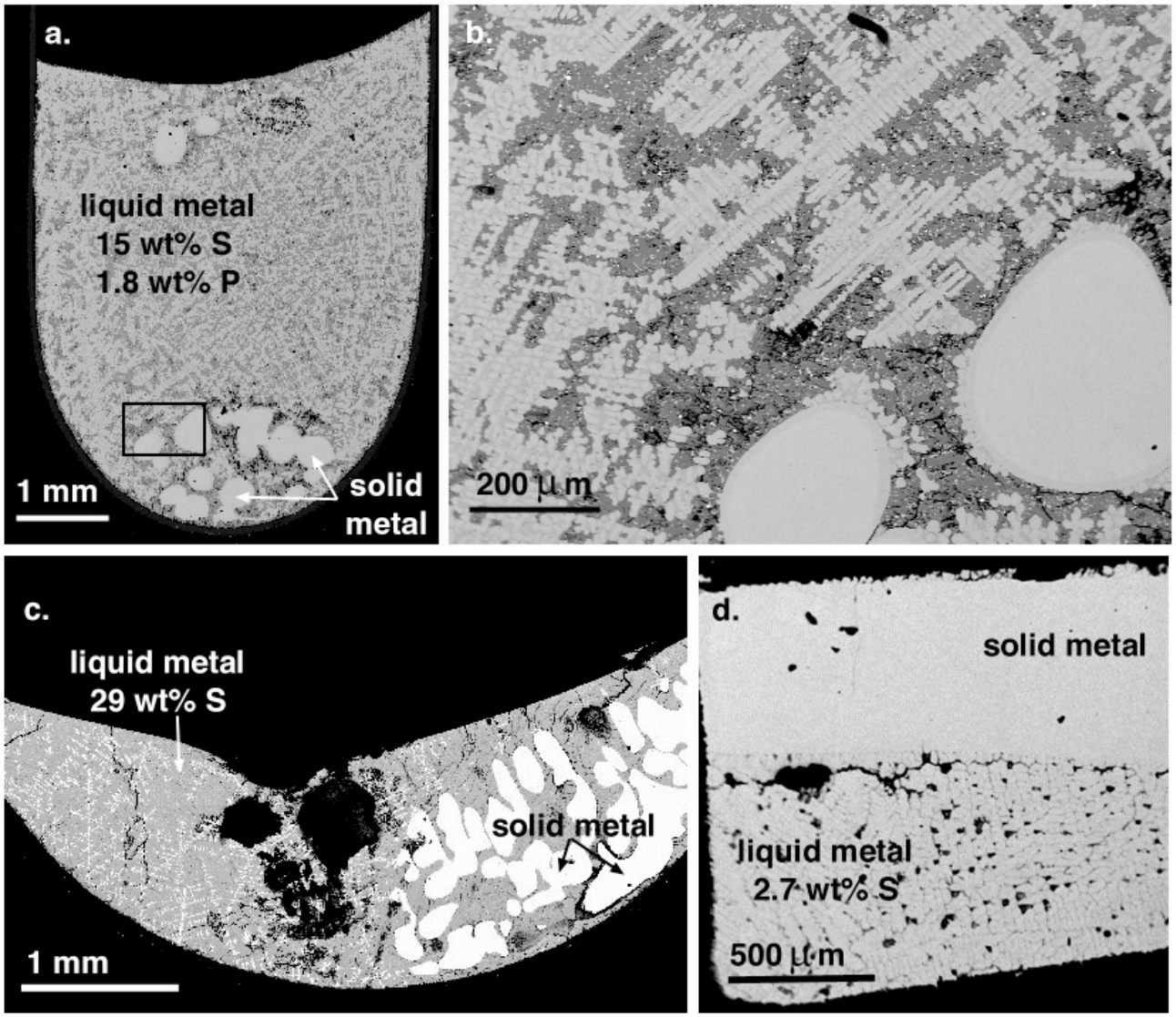


Fig. 1 Chabot et al.
An Experimental Test of Henry's Law

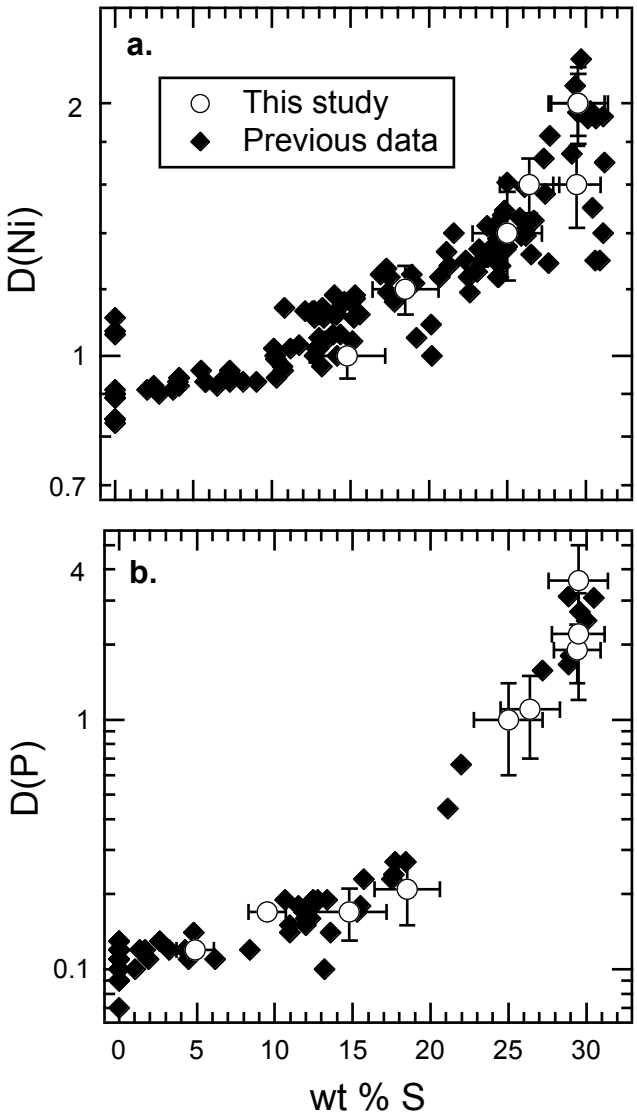


Fig. 2
Chabot et al.
An Experimental Test of Henry's Law

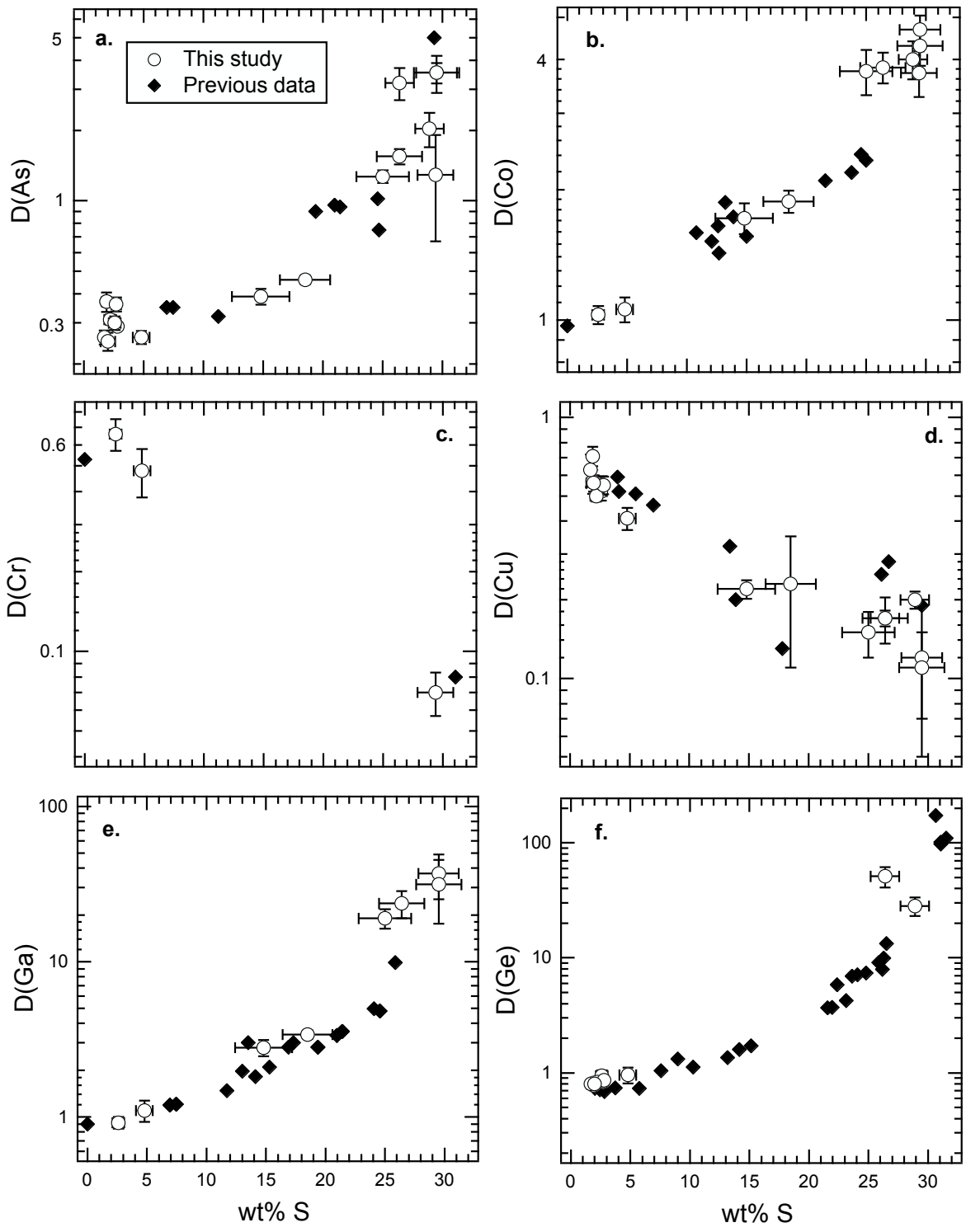


Fig. 3, Chabot et al., An Experimental Test of Henry's Law

Fig. 3 continued, Chabot et al., An Experimental Test of Henry's Law

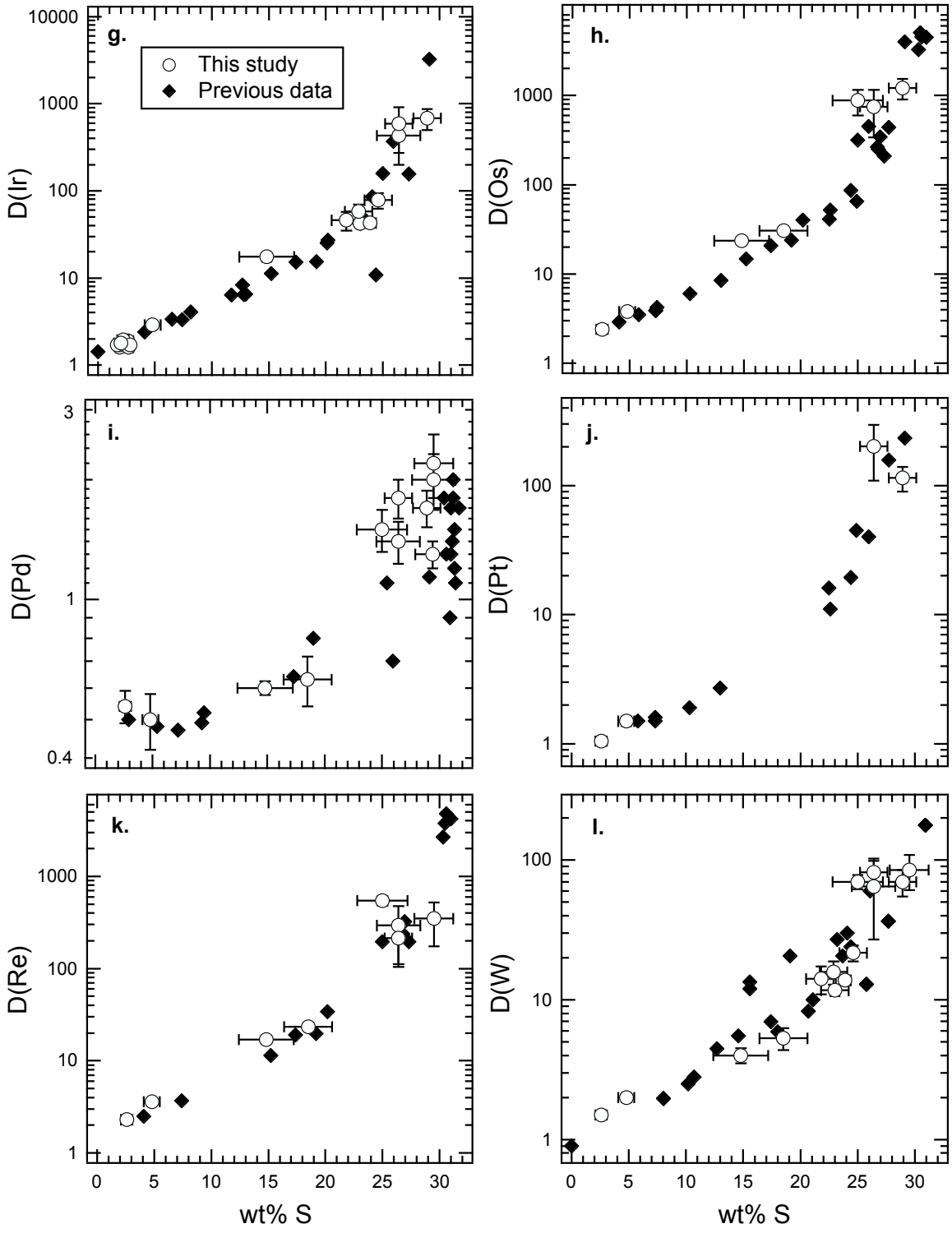

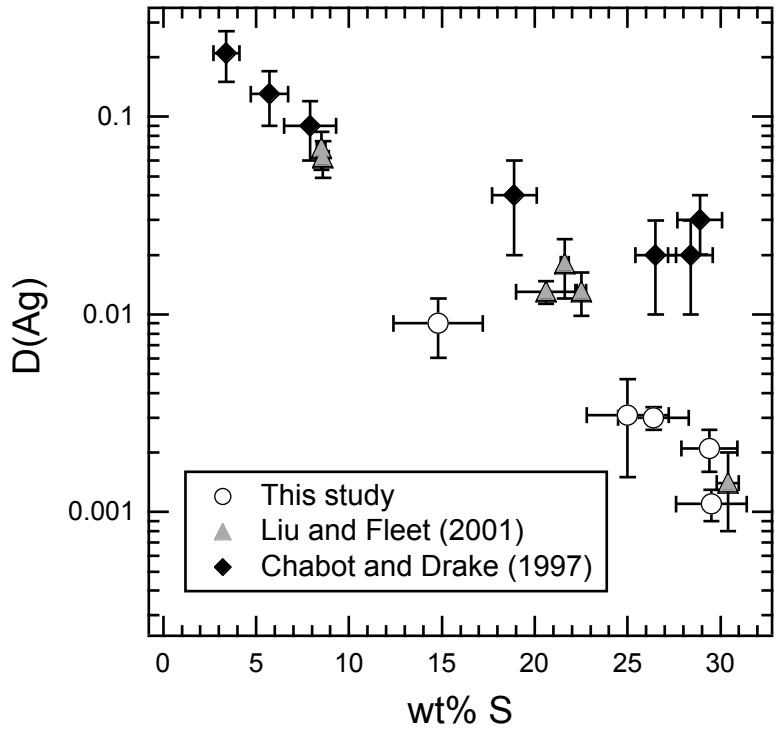


Fig. 4
Chabot et al.
An Experimental Test of Henry's Law

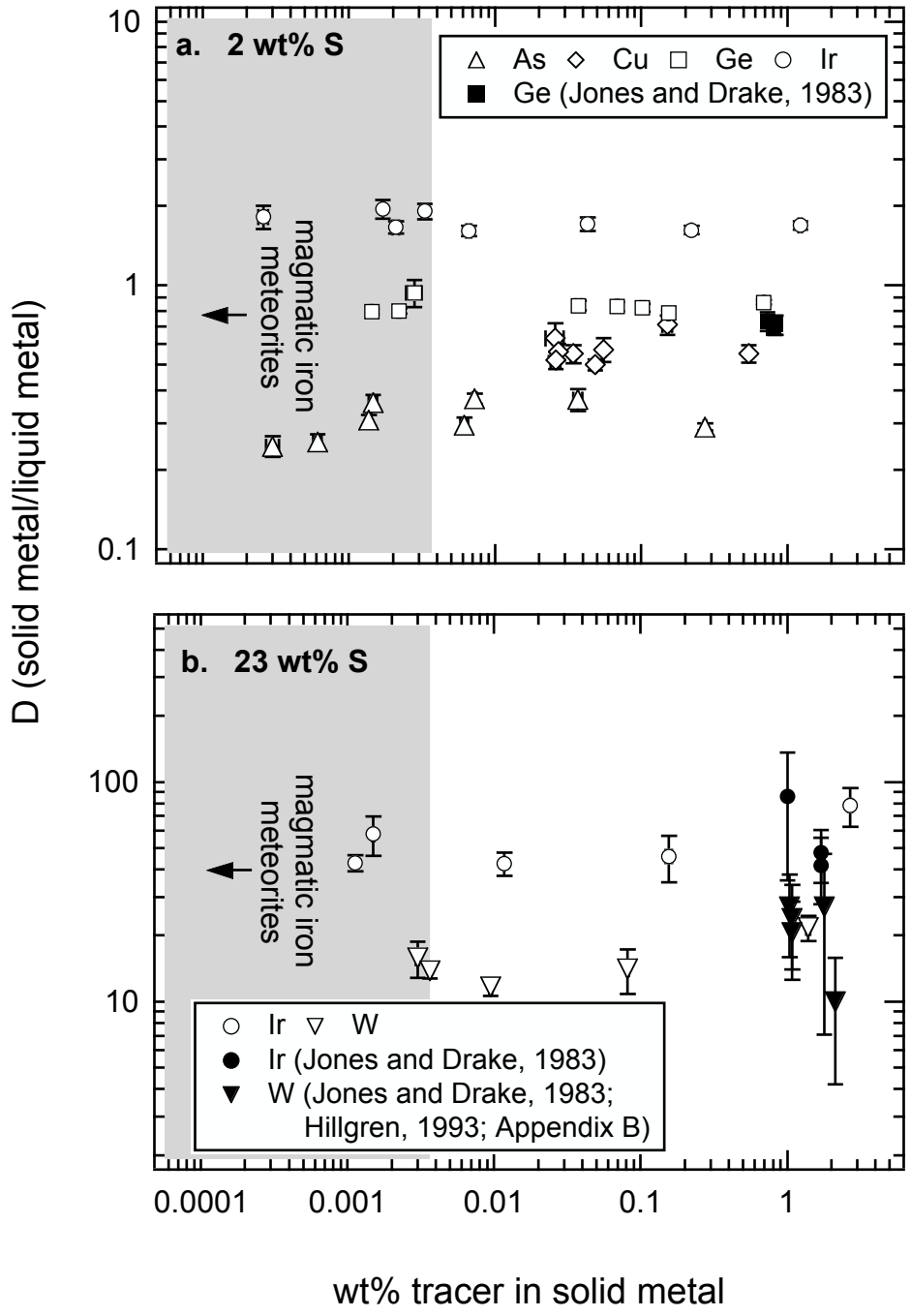


Fig. 5
Chabot et al.
An Experimental Test of Henry's Law

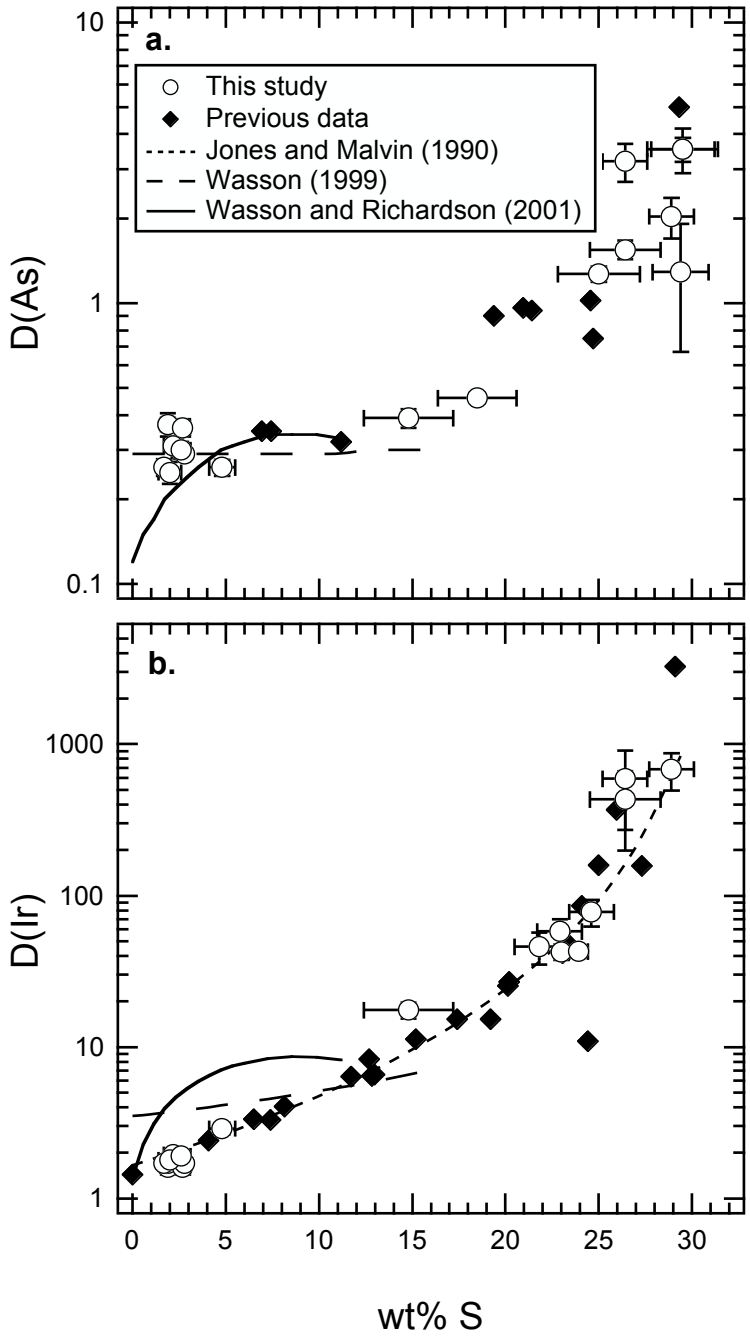


Fig. 6
Chabot et al.
An Experimental Test of Henry's Law